Photogeneration Quantum Yield and Character of Free Charges and Excitons in PbSe Nanorods

Kulkarni, Aditya; Evers, Wiel H.; Van Waas, Thomas P.; Siebbeles, Laurens D.A.

DOI
10.1021/acs.jpcc.0c00541

Publication date
2020

Document Version
Final published version

Published in
Journal of Physical Chemistry C

THE JOURNAL OF PHYSICAL CHEMISTRY C

pubs.acs.org/JPCC

Article

Photogeneration Quantum Yield and Character of Free Charges and Excitons in PbSe Nanorods

Aditya Kulkarni, Wiel H. Evers, Thomas P. van Waas, and Laurens D. A. Siebbeles*

Cite This: J. Phys. Chem. C 2020, 124, 7550–7557

Read Online

ACCESS | Metrics & More | Article Recommendations | Supporting Information

ABSTRACT: Lead selenide (PbSe) nanorods are of interest for applications in infrared LEDs, lasers, and photovoltaics due to the possibility of tuning their band gap from the far- to the near-infrared by decreasing their radius. We study the photogeneration quantum yield and properties of free charges and excitons in PbSe nanorods using a combination of time-resolved transient optical absorption and terahertz spectroscopy. Photoexcitation predominantly leads to the formation of excitons and to a smaller extent to free mobile charges. Theoretical analysis of the exprimental data yields an exciton polarizability of 10^{-35} C m^2 V^{-1}. The sum of the mobilities of a free electron and a hole is found to be close to 100 cm^2 V^{-1} s^{-1}. The high quantum yield of excitons makes PbSe nanorods of interest as a gain material in near-infrared LEDs or lasers. To use PbSe nanorods in photovoltaics, heterojunctions must be realized so that excitons can dissociate into free charges.

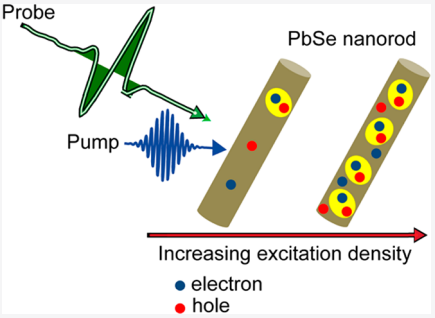

INTRODUCTION

Nanorods of PbSe are of interest due to the possibility of tuning their band gap from the far- to the near-infrared by a decrease in their radius. A band gap of close to 1 eV can be realized, which is ideal for solar cells, near-infrared detectors, and lasers.[1−3] Interestingly, it has been found that a single energetic photon can excite two or more electrons in PbSe nanorods via a process known as carrier multiplication (CM).[1,4] The effect of CM in solar cells based on PbSe nanorods was found to lead to an external quantum efficiency of close to 120%.[2]

For optoelectronic applications as mentioned, it is important to understand to what extent photon absorption leads to the formation of free electrons and holes or mutually bound electrons and holes in the form of neutral excitons. The quantum yield of excitons first increases when the photoexcitation density increases since then it becomes more likely that electrons and holes recombine to form excitons, as described by the Saha model.[5−7] At very high density where the distance between excitons becomes comparable to their diameter, their spatial overlap causes screening of the electron−hole (e−h) Coulomb attraction, which can lead to the dissociation of excitons into free charges forming an e−h plasma.[6,8] Understanding the nature of photoexcited species as a function of density is of interest from a fundamental perspective as well as for optoelectronic applications of PbSe nanorods.

Theoretical calculations on PbSe nanowires have yielded exciton binding energies that strongly increase as their radius decreases, with a value that is as high as 0.4 eV for a radius near 1 nm.[9] Transient optical absorption (TA) and photoluminescence measurements do not directly reveal to what extent photoexcitation leads to the formation of neutral excitons and free charges.[1,4,10] However, according to the theoretical analysis of TA decay kinetics, excitons are the dominant species in longer PbSe nanorods.[10,11]

The aim of the current work is to determine to what extent the photoexcitation of PbSe nanorods leads to free charges or excitons and to determine the charge carrier mobility and the exciton polarizability. We combine time-resolved TA spectroscopy with terahertz (THz) photoconductivity measurements for different photoexcitation densities in order to distinguish free charges from excitons. From an analysis of the TA and THz photoconductivity data, it is inferred that photoexcitation predominantly leads to the formation of excitons with a polarizability of 10^{-35} C m^2 V^{-1}. The quantum yield of photogenerated free charges is less than 0.13. The sum of the mobility of an electron and hole moving in phase with the THz electric field is as high as 91 ± 13 cm^2 V^{-1} s^{-1}.

METHODS

Synthesis and Characterization of Nanorods. PbSe nanorods were synthesized by exactly following a previously reported procedure.[12] Transmission electron microscopy (TEM) images were acquired using a Philips CM30T microscope operating at 200 kV. The nanorods were dispersed

Received: January 20, 2020
Revised: March 10, 2020
Published: March 16, 2020

https://dx.doi.org/10.1021/acs.jpcc.0c00541
J. Phys. Chem. C 2020, 124, 7550−7557

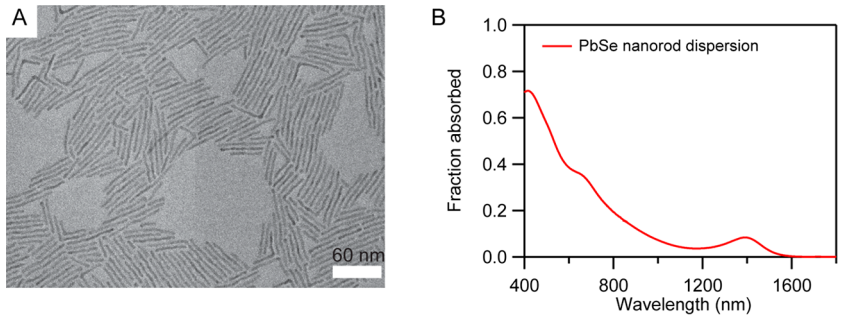

Figure 1. Structural and optical characterization. (A) TEM image of PbSe nanorods. (The scale bar represents 60 nm.) (B) Optical absorption spectrum of the PbSe nanorod dispersion exhibiting a low-energy absorption peak at 1395 nm.

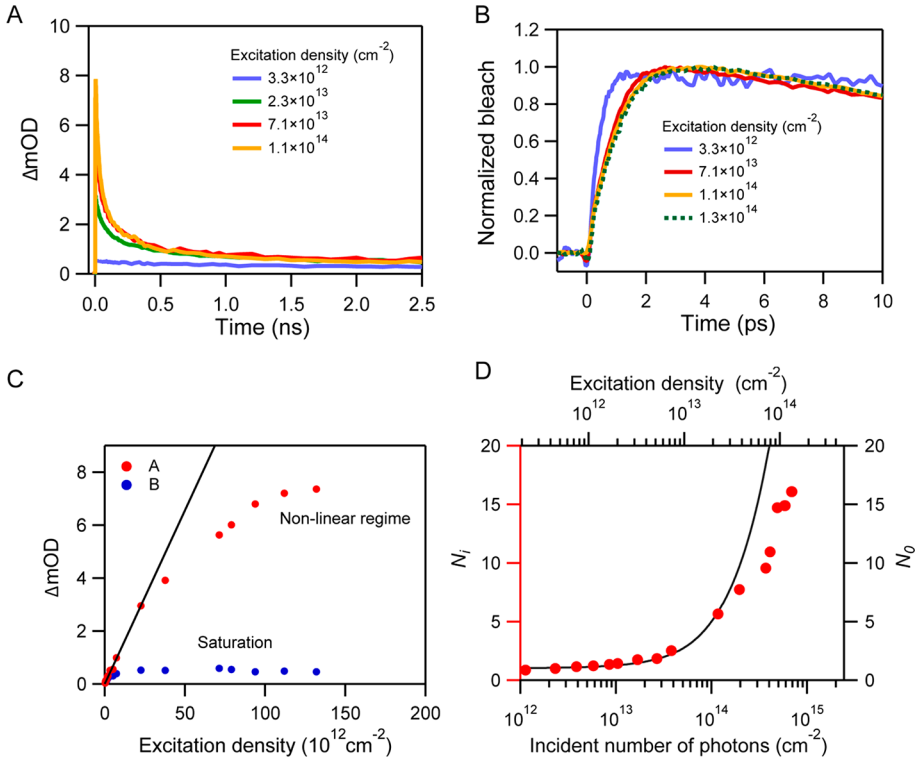

Figure 2. TA spectroscopy results. (A) ΔOD after photoexcitation at 800 nm. (B) The bleach rises more slowly at higher excitation density. (C) Initial bleach signal, *A*, obtained by averaging over a time range of 5−10 ps and the long-time bleach, *B*, obtained by averaging over 2.0−2.5 ns plotted versus the excitation density. (D) Values of $N_i = A/B$ (red markers plotted on the left axis) and N_0 (black curve plotted on the right axis) as a function of the number of incident photons per cm^2, j_0, (bottom axis) and the excitation density (top axis).

in tetrachloroethylene for all spectroscopic measurements. The steady-state optical absorption was measured using a PerkinElmer Lambda 1050 spectrophotometer.

In the pump−probe laser experiments described below, it was found that stirring the sample solution or the prolonged duration of the measurements had no effect on the results. This implies that the pump pulses do not cause charging or degradation of the nanorods.

Transient Optical Absorption Spectroscopy. The PbSe nanorod dispersion was photoexcited with 800 nm optical pulses with a duration of 180 fs. The reduced absorption (bleach) near the band gap due to presence of free electrons, holes, and excitons was probed by broadband optical pulses generated in a sapphire crystal using the laser system described in ref 12. The bleach of the low-energy absorption peak (Figure S2) was obtained from the transmitted probe light in the presence of the pump pulse (I_{on}) and the absence of the pump pulse (I_{off}) using the relation[13]

$$\Delta OD = \log\left(\frac{I_{on}(\lambda)}{I_{off}(\lambda)}\right) \quad (1)$$

The decay kinetics of the bleach was obtained by integrating the entire peak in the 1100−1600 nm interval at each pump−probe delay time.

Optical Pump−THz Probe Spectroscopy. The PbSe nanorod dispersion was photoexcited with 800 nm optical pump pulses of 60 fs width. The photogenerated free electrons, holes, and excitons were probed by single-cycle THz pulses. Single-cycle THz pulses were generated in a nonlinear crystal ZnTe via optical rectification of 60 fs pulses of wavelength 800 nm similar to that in previous work.[14,15] The THz pulse was detected in a ZnTe crystal by spatially overlapping it with a chirped optical laser pulse centered at 800 nm so that the

https://dx.doi.org/10.1021/acs.jpcc.0c00541
J. Phys. Chem. C 2020, 124, 7550−7557

entire THz waveform is detected by a single laser shot.[14,15] Differential THz signal $\Delta E(\omega, t)$ at time t after the pump pulse was obtained from the Fourier transform electrical field of the transmitted THz pulse in the presence and absence ($E_0(\omega)$) of optical pumping. The complex THz conductivity, ($\Delta\sigma$), is related to differential THz signal $\Delta E(\omega, t)$ according to[14,16,17]

$$\frac{\Delta E(\omega, t)}{E_0(\omega)} = \frac{L\Delta\sigma}{2n_{sol}c\varepsilon_0} \quad (2)$$

with L being the sample thickness, n_{sol} = 1.5 being the refractive index of the solvent, c being the speed of light in a vacuum, and ε_0 being the vacuum permittivity.

The real part of the THz conductivity signal, $S_R(t)$, is related to the quantum yield (i.e., the number of pairs of free electrons and holes per absorbed photon, $\phi(t)$, present at time t after the pump pulse) and the sum of the real component of the electron and hole mobility $\mu_e + \mu_h \equiv \mu_R$ of charges moving along the direction of the nanorod according to[7,14,16,18]

$$S_R(t) = \phi(t)\mu_R = R\frac{L\Delta\sigma_R}{eN_a} \quad (3)$$

In eq 3, e is the elementary charge and N_a is the number of absorbed photons per unit area in the nanorod dispersion, which is referred to as the photoexcitation density. Factor R in eq 3 takes into account the effects of the angle between the polarization direction of the pump laser pulse and the direction of the THz electric field with respect to the randomly oriented axes of the nanorods. The transition dipole moment for an optical transition is parallel or perpendicular to the axis of the nanorod, so the optical absorption cross section of a nanorod depends on the angle Θ of its axis with respect to the pump polarization direction according to $\cos^2(\Theta)$ or $\sin^2(\Theta)$, respectively. Assuming that the THz conductivity perpendicular to the axis of a nanorod is negligible, the THz conductivity of a nanorod at an angle Ω with the THz field is proportional to $\cos^2(\Omega)$. Taking this into account, the factor R can be determined from the ratio of the THz conductivity measured with the pump laser polarization parallel and perpendicular to the THz field, respectively. From such measurements, it was found that R = 3.3 (SI section 1). The imaginary conductivity signal $S_I(t)$ due to free electrons and holes, as well as the polarizability of excitons along the direction of the nanorod, is given by[7,18]

$$S_I(t) = \phi(t)\mu_I + [1 - \phi(t)]\frac{\alpha\omega}{e} = R\frac{L\Delta\sigma_I}{eN_a} \quad (4)$$

with μ_I being the sum of the imaginary electron and hole mobility, α being the polarizability of an exciton, and ω being the radian frequency of the THz field.

RESULTS AND DISCUSSION

According to an analysis of the TEM image in Figure 1A, the nanorods have a diameter of 4.0 ± 0.8 nm and a length of 51 ± 11 nm. The optical absorption spectrum of the PbSe nanorod dispersion is shown in Figure 1B. The absorption peak at lower photon energy is maximized at 1395 nm.

Transient Optical Absorption Spectroscopy. Figure 2A shows the time-dependent bleach, ΔOD, after photoexciting the PbSe nanorod dispersion with 800 nm pump pulses with a duration of 180 fs (Methods and Figure S2). As expected, the initial amplitude of the bleach increases with the excitation density (defined as the number of absorbed pump photons per unit area in the nanorod dispersion), while the decay becomes faster (additional data in Figure S3). The faster decay at higher density is due to Auger recombination, which occurs when multiple e−h pairs and/or excitons are present in a nanorod.[4,10,11,19] The remaining bleach at longer times is due to a single free e−h pair or a single neutral exciton in a nanorod, which decay on a longer time scale than considered here.[11,20]

Figure 2B shows the bleach normalized to the maximum value in a short time range of 5−10 ps. The rise of the bleach during this time is due to energetic relaxation (cooling) of the initially hot electrons and holes to the band edge. At the lowest excitation density, this is observed to occur within 1 ps, similar to previous results.[10] With increasing density, cooling appears to be prolonged and takes about 4 ps at the highest density. This can be understood as follows.[21] Net cooling of the charge carrier population occurs by the emission of phonons. At a higher charge carrier density, a larger number of phonons is emitted, and the nuclear lattice heats up more than for a low charge carrier density. Consequently, at higher density the reabsorption of phonons by charge carriers is more likely and the cooling time becomes longer.

The initial average number of free e−h pairs and excitons can be determined from the ratio of the maximum bleach amplitude, A, at short time after photoexcitation and the bleach at long time, B, when Auger recombination is complete and a single e−h pair or exciton is left in a photoexcited nanorod.[4,22,23] In Figure 2C, values of A are shown, as obtained by averaging the bleach over a time range of 5−10 ps, which is sufficiently long after the pump pulse so that charges have cooled to the band edge. The values of B in Figure 2C were obtained by averaging over 2.0−2.5 ns, during which the bleach in Figure 2A can be attributed to single e−h pairs or excitons since the bleach exhibits no significant decay. The values of A first increase linearly with excitation density, reflecting that the number of e−h pairs and excitons is directly proportional to the excitation density. At higher excitation density, the increase becomes sublinear, which is attributed to decay by Auger recombination on a time scale shorter than 10 ps. The value of B first increases with excitation density due to the fact that more nanorods are photoexcited, while it eventually saturates when all nanorods are excited and thus contains one e−h pair or exciton at longer times.

Figure 2D shows ratio A/B as a function of the incident (bottom axis) and absorbed (top axis) number of photons per unit area. The ratio A/B is equal to the average initial number, N_i, of e−h pairs and excitons per photoexcited nanorod in the time range of 5−10 ps. The value of N_i is equal to the average number of absorbed photons per photoexcited nanorod, N_0, provided the density of e−h pairs and excitons in the nanorods is low enough that Auger recombination at times of less than 10 ps is insignificant. The number of absorbed photons per nanorod follows a Poisson distribution so that the average initial number of e−h pairs and excitons per nanorod is equal to $j_0\sigma_{abs}$, with j_0 being the number of incident pump photons per unit area and σ_{abs} being the absorption cross section at a pump wavelength of 800 nm. The initial average number of e−h pairs and excitons per photoexcited nanorod is then equal to

$$N_0 = \frac{j_0\sigma_{abs}}{(1 - e^{-j_0\sigma_{abs}})} \quad (5)$$

https://dx.doi.org/10.1021/acs.jpcc.0c00541
J. Phys. Chem. C 2020, 124, 7550−7557

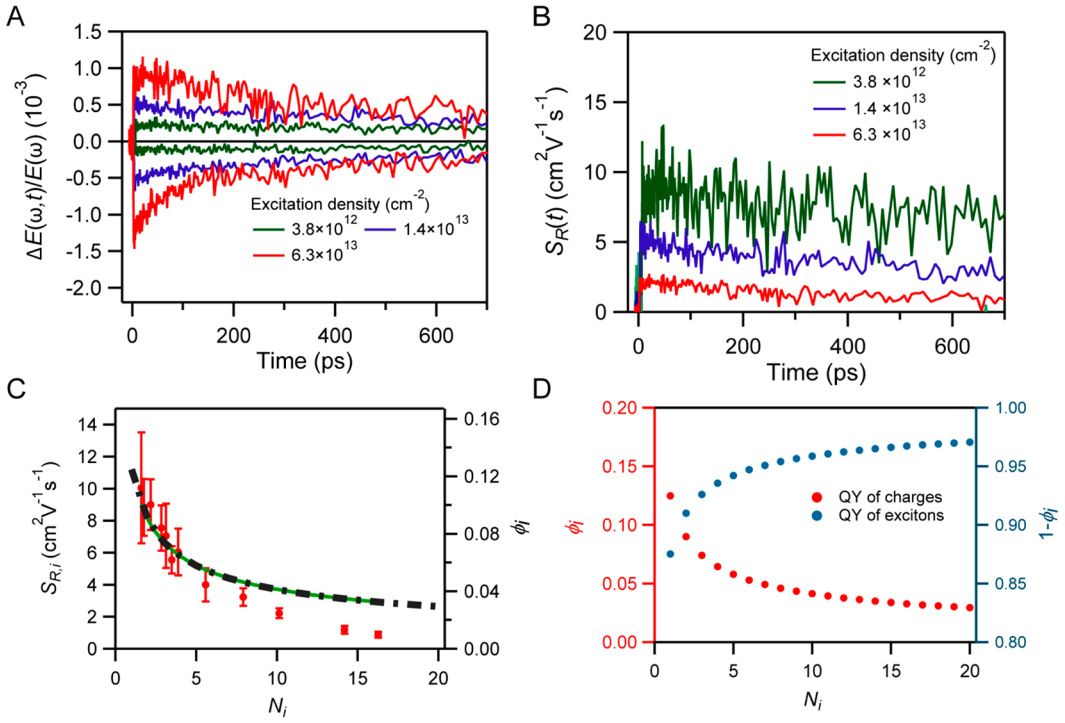

Figure 3. THz photoconductivity results. (A) Real (positive) and imaginary (negative) differential THz signals after photoexcitation at 800 nm for excitation densities as indicated. (B) Quantum-yield-weighted real mobility of free charges obtained from the data in Figure 3A. (C) Initial quantum-yield-weighted real mobility of charges, $S_{R,i}$ (red markers), and product of the quantum yield calculated from the Saha model and the fitted mobility of charges. (D) Quantum yields of charges and excitons versus N_i calculated from the Saha model.

Fitting eq 5 to the ratio A/B for those densities at which A increases linearly with the excitation density (so that Auger recombination does not affect A) yields the black curve in Figure 2D with $\sigma_{abs} = (5.0 \pm 0.4) \times 10^{-14}$ cm^2. At higher excitation density, A/B is smaller than N_0, which is attributed to the decay of e−h pairs and excitons by Auger recombination on a time scale shorter than 10 ps.

For the value of σ_{abs} at 800 nm obtained from the fit, the optical absorption spectrum in Figure 1B yields an absorption cross section at the maximum of the low-energy peak equal to 2×10^{-14} cm^2. Cunningham et al. reported a cross section of 7.2×10^{-15} cm^2 at the low-energy peak for PbSe nanorods with volume 240 nm^3.[19] Taking our value of σ_{abs} at the low-energy peak and assuming it to scale linearly with the nanorod volume,[24] which is 640 nm^3 for our nanorods,[4,19] yields an absorption cross section of 7.5×10^{-15} cm^2 for nanorods of volume 240 nm^3, which agrees with the value reported by Cunningham et al.[19]

THz Spectroscopy. THz photoconductivity experiments were conducted to determine to what extent photoexcitation leads to the formation of free e−h pairs and neutral excitons. Figure 3 shows THz photoconductivity data obtained by photoexcitation of the PbSe nanorods with 800 nm pump pulses of 60 fs duration. The real component of the THz conductivity is due to the motion of charges with velocity in phase with the THz field, and the imaginary part of the THz conductivity is due to the out-of-phase velocity resulting from the backscattering of charges and the polarizability of excitons (Methods).[16,17,25]

Figure 3A shows the real (positive) and imaginary (negative) components of the differential THz signal averaged over frequencies ($f = \omega/2\pi$) in the range of 0.5−1.2 THz as a function of time after the pump pulse. To realize the absorption of at most one photon per nanorod, it was necessary to use low excitation densities, leading to a relatively large noise level in the THz signals. The differential THz signal is directly proportional to the conductivity or, equivalently, the density of e−h pairs and excitons weighted by their mobility and polarizability, respectively (Methods). The real component is attributed to the presence of free mobile charge carriers only. Excitons do not contribute to the real component since the calculated exciton binding energy in PbSe nanowires of diameter 4 nm is as high as 0.154 eV (ref 9); consequently, excitation to a higher exciton level will largely exceed the THz photon energy (1 THz = 4 meV). At higher excitation density, the imaginary THz signal decays faster than the real component. This must be due to the fact that excitons also contribute to the imaginary component. Hence, from the data in Figure 3A, we can conclude that both e−h pairs and excitons are produced by photoexcitation.

Figure 3B shows the real component of the product of the quantum yield of e−h pairs, $\phi(t)$, and the sum of the mobility of an electron and a hole (i.e., $S_R(t) = \phi(t)\mu_R$). Note that the quantum yield is the number of e−h pairs per absorbed pump photon at time t after the pump pulse. It can be seen that S_R decays faster at higher excitation density, which is due to the enhanced Auger recombination of charges. The reduction of the magnitude of S_R with excitation density may result from a decrease in the quantum yield of charges and/or a reduction in the charge mobility at higher density. This reduction will be addressed further in the next section. The initial values of the quantum-yield-weighted real mobility, $S_R(t)$, averaged over t in the interval 5−10 ps are shown in Figure 3C as a function of the average initial number of e−h pairs and excitons per nanorod, N_i.

https://dx.doi.org/10.1021/acs.jpcc.0c00541
J. Phys. Chem. C 2020, 124, 7550−7557

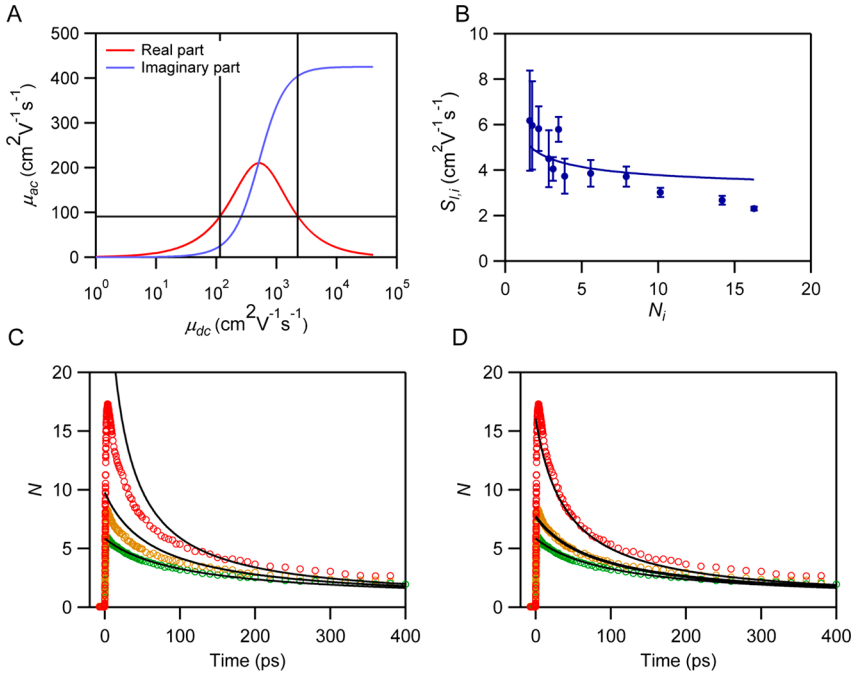

Figure 4. Theoretical modeling. (A) Calculated real and imaginary components of μ_{ac} as a function of μ_{dc} at frequency 0.8 THz for a nanorod of length 51 nm. (B) Experimental $S_{I,i}$ values (markers), obtained by averaging over 5−10 ps after the laser pump pulse and fit with μ_I = 25 cm^2 V^{-1} s^{-1} and α as an adjustable parameter (drawn curve). (C) Experimental (markers) and theoretical (drawn black curves) decays of N as a function of time with the initial condition for a Poisson distribution of excitons; see eq 10. (D) Decay with $N = N_i$ as the initial condition in eq 10 for $N \geq 6$.

Quantum Yield and Mobility of Charges and Polarizability of Excitons. According to the 1D Saha model, the equilibrium between the density of pairs of free charges $n_q = \phi_i N_i/L$ and excitons $n_X = (1 - \phi_i)N_i/L$ on a nanorod of length L is described by[26]

$$\frac{n_q^{\,2}}{n_X} = K = \left(\frac{2m^* k_B T}{\pi\hbar^2}\right)^{1/2} \exp\left(\frac{-E_X}{k_B T}\right) \tag{6}$$

The quantum yield of e−h pairs ϕ_i is obtained from the real THz conductivity data 5−10 ps after the pump pulse in Figure 3C. The reduced effective mass of electrons and holes $m = 0.112m_0$ is obtained from the calculated valence and conduction band dispersion (SI Section 5) reported in the literature,[9] and the exciton binding energy E_X = 0.154 eV is also taken from the literature.[9] k_B is the Boltzmann constant, $\hbar$ is the reduced Planck constant, and T is the temperature (293 K). Using eq 6, the quantum yield of e−h pairs is found to be $\phi_i = \frac{-KL}{2N_i}\left(1 - \sqrt{1 + \frac{4N_i}{KL}}\right)$. Fitting the product $\phi_i\mu_R$ to the data in Figure 3C with K calculated from eq 6 and the mobility of an e−h pair as an adjustable parameter yields $\mu_R = 91 \pm 13$ cm^2 V^{-1} s^{-1}. The fit reproduces the experimental values of $S_{R,i}$ up to $N_i = 6$. The reduction of $S_{R,i}$ with N_i can be attributed to a decrease in the quantum yield of e−h pairs (and thus higher quantum yield of excitons), as described by the Saha model (eq 6). Note that filling of traps with charges would lead to an increase in $S_{R,i}$ when N_i increases. Hence, trap filling is not important. For higher values of N_i, the experimental values of $S_{R,i}$ are lower than those from the fit. This can be due to a decrease in the charge mobility since at higher density the mutual scattering of charges in a rod of finite length will reduce their mobility. Figure 3D shows the quantum yield of e−h pairs and that of excitons. It is seen that photoexcitation leads mainly to the formation of excitons with a quantum yield exceeding 0.85 even at low N_i.

The real mobility of charges obtained above can be limited by scattering at the ends of the nanorod. The alternating current (AC) charge carrier mobility $\mu_{ac}(f)$ at THz frequency f on a nanorod of finite length L can be related to the direct current (DC) mobility μ_{dc} of a charge on an infinitely long nanowire according to[27−29]

$$\mu_{ac}(f) = 8\mu_{dc}\sum_{p=0}^{\infty}\frac{C_p^{-2}}{1 - \frac{ik_B T\mu_{dc}}{eL^2 2\pi f}C_p^{\,2}} \tag{7}$$

with e being the elementary charge and $C_p = 2\pi\left(p + \frac{1}{2}\right)$.

Equation 7 yields for the real and imaginary components

$$\mu_{ac}^{R}(f) = 8\mu_{dc}\sum_{p=0}^{\infty}\frac{C_p^{-2}}{1 + \left(\frac{k_B T\mu_{dc}}{eL^2 2\pi f}\right)^2 C_p^{\,4}} \tag{8}$$

$$\mu_{ac}^{I}(f) = 8\mu_{dc}\sum_{p=0}^{\infty}\frac{C_p^{-2}\frac{k_B T\mu_{dc}}{eL^2 2\pi f}}{1 + \left(\frac{k_B T\mu_{dc}}{eL^2 2\pi f}\right)^2 C_p^{\,4}} \tag{9}$$

Figure 4A shows the real and imaginary parts of the ac mobility for f = 0.8 THz (the central frequency at which the experimental data in Figures 3 and 4 were obtained) calculated from eqs 8 and 9 for a nanorod length of L = 51 nm as a function of μ_{dc}. The experimental AC mobility is reproduced for 115 and 2265 cm^2 V^{-1} s^{-1}. The correct value can be determined by also considering the initial imaginary THz conductivity data in Figure 4B, which correspond to $S_{I,i} = \phi_i\mu_I + [1 - \phi_i]\frac{\alpha\omega}{e}$ (eq 4), with μ_I being the sum of the imaginary electron and hole mobility, α being the

https://dx.doi.org/10.1021/acs.jpcc.0c00541
J. Phys. Chem. C 2020, 124, 7550−7557

polarizability of an exciton, and ω being the radian frequency of the THz field. Fitting $S_{I,i}$ with the quantum yield from the Saha model and μ_I = 25 cm^2 V^{-1} s^{-1} (corresponding to μ_{dc} = 115 cm^2 V^{-1} s^{-1}) yields the drawn curve in Figure 4B with α = (0.9 ± 0.1) × 10^{-35} C m^2 V^{-1}. The fit reproduces the experimental data with the exception of high densities. By contrast, taking μ_{dc} = 2265 cm^2 V^{-1} s^{-1} and the corresponding μ_I = 404 cm^2 V^{-1} s^{-1} fails to reproduce the measured data (Figure S6). Therefore, we conclude that μ_{dc} = 115 cm^2 V^{-1} s^{-1}. Since this value is close to the measured real THz mobility, the effect of scattering of charges at the ends of a nanorod is very small when probed at a frequency near 0.8 THz. The mobility from the present work is comparable to that reported previously for as-grown colloidal PbSe nanowires in a field-effect transistor device.[30] Interestingly, the mobility in the device could be enhanced by about an order of magnitude via coating the nanowires with SiO_2.[30] Unfortunately, after being coated the nanowires are no longer solution processable. The mobility of charges in the colloidal PbSe nanorods is more than 1 order of magnitude higher than for amorphous silicon, making the nanorods of interest for electronic applications.

In the analysis described above, it was assumed that either the electron or the hole is mobile, which gives a lower limit to the exciton polarizability. Since the effective masses of electrons and holes are almost equal (SI Section 5), it is reasonable to assume that electrons and holes have the same mobility of 45 cm^2 V^{-1} s^{-1}. In that case, we obtain μ_I = 12 cm^2 V^{-1} s^{-1} and an upper limit to the exciton polarizability equal to α = 1.1 × 10^{-35} C m^2 V^{-1}. The exciton polarizability can be estimated theoretically using $\alpha_{theory} = \frac{2e^2 a_B^2}{E_1 - E_0}$,[31] where the summation over all higher exciton states is reduced to the first only, the transion dipole moment is taken to be equal to the calculated exciton Bohr radius a_B = 2.2 nm, and $E_1 - E_2$ is taken to be equal to the exciton binding energy for PbSe nanowires with 4 nm diameter, as mentioned above.[9] This gives α_{theory} = 10^{-35} C m^2 V^{-1}, which is in close agreement with the experimental result of (1.0 ± 0.1) × 10^{-35} C m^2 V^{-1}. The agreement between the experimental polarizability and that theoretically estimated from the calculated Bohr radius and exciton binding energy supports the validity of the theoretical model for the electronic structure used in ref 9. The much smaller Bohr radius than for bulk PbSe (46 nm)[9] is attributed to geometrical confinement in a nanowire and the lower dielectric constant of the surrounding medium (i.e., the surface ligands and the solvent).

As discussed above, photoexcitation of the PbSe nanorods leads mainly to excitons (Figure 3D). Hence, the optical bleach at the band gap (ΔOD in Figures 2A, S2, and S3) can lead to a good approximation taken as a measure of the average number of excitons per nanorod, which we denote as N. As discussed above, for low excitation densities $N_i = N_0 \leq 6$, the maximum bleach at short time directly reflects the average number of photoexcitations per nanorod. For these densities, the transients in Figure 4C,D were obtained by scaling the measured bleach (ΔOD) such that they have magnitude $j_0\sigma_{abs}$ at the maximum. At higher densities, this procedure is not valid due to Auger recombination of hot charge carriers prior to having relaxed to the band gap. This causes the maximum bleach at short time to be smaller than $j_0\sigma_{abs}$, as seen in Figure 2D. Fortunately, at these higher densities all nanorods are photoexcited and the bleach can be scaled such that at long times N = 1.

Taking into account the Auger recombination of excitons, the time-dependent average number of excitons per nanorod is given by[32]

$$N(t) = \sum_{i=1}^{\infty} A_i \exp\left[- i\left(\frac{1}{2}(i-1)k_2^A\right)t\right] \quad (10)$$

with k_2^A being the Auger recombination rate for two excitons in a nanorod. The coefficients in eq 10 are equal to[32]

$$A_i = N^i e^{-N}(2i-1)\sum_{j=0}^{\infty}\frac{N^j}{j!}\frac{\Gamma(i+j)}{\Gamma(2i+j)} \quad (11)$$

By taking the initial value of the number of photogenerated excitons in a nanorod equal to $N = j_o\sigma_{abs}$, we could reproduce the measured optical bleach transients until N = 6 with a value of k_2^A = 3 × 10^9 s^{-1} (Figure 4C). For N > 6, the fitted transients exceed the experimental results at shorter times. This is attributed to the Auger recombination of hot e−h pairs before they reach the band edge so that the maximum in the measured transient does not represent the initial number of photoexcitations. Hence, for the transients at higher density such that N > 6, we take N_i from Figure 2D as the initial value N in eq 11, yielding the curves shown in Figure 4D. The fitted curves in Figure 4D obtained with k_2^A = 3 × 10^9 s^{-1} agree with the experimental data. From this, we infer that the Auger recombination of hot e−h pairs reduces the initial average number of excitons at the band gap in a nanorod while approximately maintaining a Poisson distribution, which is the initial condition for eq 10. Results for other densities are shown in Figure S7. The biexciton lifetime of $1/k_2^A$ = 330 ps obtained as described above is somewhat longer than the value of 210 ps reported for shorter nanorods of average length 25 and 4 nm diameter.[10] This can be understood since in longer nanorods the spatial overlap between two excitons will be smaller than in shorter nanorods, which enhances the lifetime before Auger recombination.

CONCLUSIONS

Photoexcitation of the PbSe nanorods studied predominantly leads to excitons rather than free e−h pairs. The exciton polarizability of 10^{-35} C m^2 V^{-1} inferred from the experiments agrees with the polarizability from a theoretical estimate. The sum of the mobility of an electron and hole moving in phase with the THz electric field is as high as 91 ± 13 cm^2 V^{-1} s^{-1}. For higher photoexcitation density, the photoconductivity is strongly affected by mutual interactions between charges and excitons, leading to a lower charge mobility. The high quantum yield of excitons makes PbSe nanorods of interest as a gain material in near-infrared LEDs or lasers. For the use of PbSe nanorods in solar cells, heterojunctions must be realized so that excitons can dissociate into free charges.

ASSOCIATED CONTENT

Supporting Information

The Supporting Information is available free of charge at https://pubs.acs.org/doi/10.1021/acs.jpcc.0c00541.

Determination of factor R in eqs 3 and 4 of the main text, spectral bleach for different values of N_i, TA spectroscopy data, THz photoconductivity data, determination of the effective masses of electrons and holes, fit to the imaginary component of the THz signal, and simulated decay of optical bleach (PDF)

https://dx.doi.org/10.1021/acs.jpcc.0c00541
J. Phys. Chem. C 2020, 124, 7550−7557

AUTHOR INFORMATION

Corresponding Author

Laurens D. A. Siebbeles − *Optoelectronic Materials Section, Department of Chemical Engineering, Delft University of Technology 2629 HZ Delft, The Netherlands;* orcid.org/0000-0002-4812-7495; Email: L.D.A.Siebbeles@tudelft.nl

Authors

Aditya Kulkarni − *Optoelectronic Materials Section, Department of Chemical Engineering, Delft University of Technology 2629 HZ Delft, The Netherlands*

Wiel H. Evers − *Optoelectronic Materials Section, Department of Chemical Engineering, Delft University of Technology 2629 HZ Delft, The Netherlands*

Thomas P. van Waas − *Optoelectronic Materials Section, Department of Chemical Engineering, Delft University of Technology 2629 HZ Delft, The Netherlands*

Complete contact information is available at: https://pubs.acs.org/10.1021/acs.jpcc.0c00541

Author Contributions

W.H.E. synthesized the samples. A.K. performed terahertz photoconductivity and transient optical absorption spectroscopy measurements. A.K. and L.D.A.S. analyzed the experimental results. T.P.v.W. provided theoretical support. L.D.A.S. supervised the work and wrote the manuscript with A.K. All authors discussed the results and commented on the manuscript.

Notes

The authors declare no competing financial interest.

ACKNOWLEDGMENTS

This work is part of the research programme of the Foundation for Fundamental Research on Matter (FOM), which is part of The Netherlands Organisation for Scientific Research (NWO) in the program "Designing Dirac Carriers in Semiconductor Honeycomb Superlattices".

REFERENCES

(1) Cunningham, P. D.; Boercker, J. E.; Foos, E. E.; Lumb, M. P.; Smith, A. R.; Tischler, J. G.; Melinger, J. S. Enhanced Multiple Exciton Generation in Quasi-One-Dimensional Semiconductors. *Nano Lett.* **2011**, *11*, 3476−3481.

(2) Davis, N. J. L. K.; Böhm, M. L.; Tabachnyk, M.; Wisnivesky-Rocca-Rivarola, F.; Jellicoe, T. C.; Ducati, C.; Ehrler, B.; Greenham, N. C. Multiple-Exciton Generation in Lead Selenide Nanorod Solar Cells with External Quantum Efficiencies Exceeding 120%. *Nat. Commun.* **2015**, *6*, 8259.

(3) Talebi, H.; Dolatyari, M.; Rostami, G.; Manzuri, A.; Mahmudi, M.; Rostami, A. Fabrication of Fast Mid-Infrared Range Photodetector Based on Hybrid Graphene−PbSe Nanorods. *Appl. Opt.* **2015**, *54*, 6386−6390.

(4) Padilha, L. A.; Stewart, J. T.; Sandberg, R. L.; Bae, W. K.; Koh, W. K.; Pietryga, J. M.; Klimov, V. I. Carrier Multiplication in Semiconductor Nanocrystals: Influence of Size, Shape, and Composition. *Acc. Chem. Res.* **2013**, *46*, 1261−1269.

(5) Kaindl, R. A.; Hägele, D.; Carnahan, M. A.; Chemla, D. S. Transient Terahertz Spectroscopy of Excitons and Unbound Carriers in Quasi-Two-Dimensional Electron-Hole Gases. *Phys. Rev. B: Condens. Matter Mater. Phys.* **2009**, *79*, 045320.

(6) Hangleiter, A.; Jin, Z.; Gerhard, M.; Kalincev, D.; Langer, T.; Bremers, H.; Rossow, U.; Koch, M.; Bonn, M.; Turchinovich, D. Efficient Formation of Excitons in a Dense Electron-Hole Plasma at Room Temperature. *Phys. Rev. B: Condens. Matter Mater. Phys.* **2015**, *92*, 241305.

(7) Lauth, J.; Kulkarni, A.; Spoor, F. C. M.; Renaud, N.; Grozema, F. C.; Houtepen, A. J.; Schins, J. M.; Kinge, S.; Siebbeles, L. D. A. Photogeneration and Mobility of Charge Carriers in Atomically Thin Colloidal Inse Nanosheets Probed by Ultrafast Terahertz Spectroscopy. *J. Phys. Chem. Lett.* **2016**, *7*, 4191−4196.

(8) Suzuki, T.; Shimano, R. Exciton Mott Transition in Si Revealed by Terahertz Spectroscopy. *Phys. Rev. Lett.* **2012**, *109*, 046402.

(9) Bartnik, A. C.; Efros, A. L.; Koh, W. K.; Murray, C. B.; Wise, F. W. Electronic States and Optical Properties of PbSe Nanorods and Nanowires. *Phys. Rev. B: Condens. Matter Mater. Phys.* **2010**, *82*, 195313.

(10) Yang, J.; Hyun, B.-R.; Basile, A. J.; Wise, F. W. Exciton Relaxation in PbSe Nanorods. *ACS Nano* **2012**, *6*, 8120−8127.

(11) Aerts, M.; Spoor, F. C. M.; Grozema, F. C.; Houtepen, A. J.; Schins, J. M.; Siebbeles, L. D. A. Cooling and Auger Recombination of Charges in PbSe Nanorods: Crossover from Cubic to Bimolecular Decay. *Nano Lett.* **2013**, *13*, 4380−4386.

(12) Placencia, D.; Boercker, J. E.; Foos, E. E.; Tischler, J. G. Synthesis and Optical Properties of PbSe Nanorods with Controlled Diameter and Length. *J. Phys. Chem. Lett.* **2015**, *6*, 3360−3364.

(13) Spoor, F. C. M.; Kunneman, L. T.; Evers, W. H.; Renaud, N.; Grozema, F. C.; Houtepen, A. J.; Siebbeles, L. D. A. Hole Cooling Is Much Faster Than Electron Cooling in PbSe Quantum Dots. *ACS Nano* **2016**, *10*, 695−703.

(14) Evers, W. H.; et al. High Charge Mobility in Two-Dimensional Percolative Networks of PbSe Quantum Dots Connected by Atomic Bonds. *Nat. Commun.* **2015**, *6*, 8195.

(15) Kulkarni, A.; Evers, W. H.; Tomić, S.; Beard, M. C.; Vanmaekelbergh, D.; Siebbeles, L. D. A. Efficient Steplike Carrier Multiplication in Percolative Networks of Epitaxially Connected PbSe Nanocrystals. *ACS Nano* **2018**, *12*, 378−384.

(16) Ulbricht, R.; Hendry, E.; Shan, J.; Heinz, T. F.; Bonn, M. Carrier Dynamics in Semiconductors Studied with Time-Resolved Terahertz Spectroscopy. *Rev. Mod. Phys.* **2011**, *83*, 543−586.

(17) Joyce, H. J.; Boland, J. L.; Davies, C. L.; Baig, S. A.; Johnston, M. B. A Review of the Electrical Properties of Semiconductor Nanowires: Insights Gained from Terahertz Conductivity Spectroscopy. *Semicond. Sci. Technol.* **2016**, *31*, 103003.

(18) Tomar, R.; Kulkarni, A.; Chen, K.; Singh, S.; van Thourhout, D.; Hodgkiss, J. M.; Siebbeles, L. D. A.; Hens, Z.; Geiregat, P. Charge Carrier Cooling Bottleneck Opens up Nonexcitonic Gain Mechanisms in Colloidal Cdse Quantum Wells. *J. Phys. Chem. C* **2019**, *123*, 9640−9650.

(19) Cunningham, P. D.; Boercker, J. E.; Placencia, D.; Tischler, J. G. Anisotropic Absorption in PbSe Nanorods. *ACS Nano* **2014**, *8*, 581−590.

(20) Schaller, R. D.; Klimov, V. I. High Efficiency Carrier Multiplication in PbSe Nanocrystals: Implications for Solar Energy Conversion. *Phys. Rev. Lett.* **2004**, *92*, 186601.

(21) Shah, J. Ultrafast Luminescence Studies of Carrier Relaxation and Tunneling in Semiconductor Nanostructures. In *Hot Carriers in Semiconductor Nanostructures*; Shah, J., Ed.; Academic Press: San Diego, 1992; pp 279−312.

(22) Trinh, M. T.; Houtepen, A. J.; Schins, J. M.; Hanrath, T.; Piris, J.; Knulst, W.; Goossens, A. P. L. M.; Siebbeles, L. D. A. In Spite of Recent Doubts Carrier Multiplication Does Occur in PbSe Nanocrystals. *Nano Lett.* **2008**, *8*, 1713−1718.

(23) Ellingson, R. J.; Beard, M. C.; Johnson, J. C.; Yu, P.; Micic, O. I.; Nozik, A. J.; Shabaev, A.; Efros, A. L. Highly Efficient Multiple Exciton Generation in Colloidal PbSe and Pbs Quantum Dots. *Nano Lett.* **2005**, *5*, 865−871.

(24) Moreels, I.; Lambert, K.; De Muynck, D.; Vanhaecke, F.; Poelman, D.; Martins, J. C.; Allan, G.; Hens, Z. Composition and Size-Dependent Extinction Coefficient of Colloidal PbSe Quantum Dots. *Chem. Mater.* **2007**, *19*, 6101−6106.

(25) Lloyd-Hughes, J.; Jeon, T.-I. A Review of the Terahertz Conductivity of Bulk and Nano-Materials. *J. Infrared, Millimeter, Terahertz Waves* **2012**, *33*, 871−925.
(26) Ambigapathy, R.; Bar-Joseph, I.; Oberli, D. Y.; Haacke, S.; Brasil, M. J.; Reinhardt, F.; Kapon, E.; Deveaud, B. Coulomb Correlation and Band Gap Renormalization at High Carrier Densities in Quantum Wires. *Phys. Rev. Lett.* **1997**, *78*, 3579−3582.
(27) Grozema, F. C.; Siebbeles, L. D. A. Mechanism of Charge Transport in Self-Organizing Organic Materials. *Int. Rev. Phys. Chem.* **2008**, *27*, 87−138.
(28) Bhaskar, P.; Achtstein, A. W.; Diedenhofen, S. L.; Siebbeles, L. D. A. Mobility and Decay Dynamics of Charge Carriers in One-Dimensional Selenium Van Der Waals Solid. *J. Phys. Chem. C* **2017**, *121*, 18917−18921.
(29) Prins, P.; Grozema, F. C.; Schins, J. M.; Patil, S.; Scherf, U.; Siebbeles, L. D. A. High Intrachain Hole Mobility on Molecular Wires of Ladder-Type Poly(Para-Phenylenes). *Phys. Rev. Lett.* **2006**, *96*, 146601.
(30) Graham, R.; Yu, D. High Carrier Mobility in Single Ultrathin Colloidal Lead Selenide Nanowire Field Effect Transistors. *Nano Lett.* **2012**, *12*, 4360−4365.
(31) Atkins, P. W.; Friedman, R. S. *Molecular Quantum Mechanics*; OUP Oxford, 2011.
(32) Barzykin, A. V.; Tachiya, M. Stochastic Models of Charge Carrier Dynamics in Semiconducting Nanosystems. *J. Phys.: Condens. Matter* **2007**, *19*, 065105.

https://dx.doi.org/10.1021/acs.jpcc.0c00541
J. Phys. Chem. C 2020, 124, 7550−7557